Iranian Journal of Materials Forming 11 (2) (2024) 62-74

Online ISSN: 2383-0042

IJMF

Iranian Journal of Materials Forming

Journal Homepage: http://ijmf.shirazu.ac.ir

Research Article

Modeling the Plastic Deformation of Dense and Porous Biomaterials Using Modified Yield Criteria by Lode Angle

K. Narooei*

Department of Materials Science and Engineering, K. N. Toosi University of Technology, Tehran, Iran

ARTICLE INFO

Article history:

Received 30 July 2024
Reviewed 7 September 2024
Revised 20 September 2024
Accepted 23 September 2024

Keywords:

Modified Gurson model (GTN)
Lode angle
Hershey-Dalgreen model
Porous materials
Biomaterials

Please cite this article as:

Narooei, K. (2024). Modeling the plastic deformation of dense and porous biomaterials using modified yield criteria by Lode angle. *Iranian Journal of Materials Forming*, *11*(2), 62-74. https://doi.org/10.22099/IJMF.2024.50853.1301

ABSTRACT

In this research, the von Mises and Gurson models were modified by incorporating the Lode angle and void volume fraction to predict the mechanical behavior of materials with non-uniform geometry or porous (cellular) structures, where the stress state affects yield behavior. The yield functions were enhanced multiplying them by a function of the Lode angle, and the Voce model was employed to account for the hardening or softening of various materials. The material parameters of the Voce model were determined by fitting the experimental data for steel, elk antler, polyurethane foam, and bioscaffold. To improve alignment with experimental data, the void volume fraction was treated as a function of the trace of the plastic strain tensor. It was observed that by varying the Lode function parameters, different shapes for the yield surface were achieved, allowing for the selection of tailored yield function for specific materials. Results of finite element (FE) constitutive modeling showed that by selecting an appropriate yield function and determining suitable values for the Lode angle function parameters, the modified yield function can accurately predict the mechanical behavior of various materials. It was observed that the barreling of porous compressed materials depends on the porosity and friction.

1. Introduction

Understanding the mechanical behavior of hard tissues, such as bones, antlers, and trabeculae is essential for preventing tissue damage and developing effective treatments. Extensive experimental research has focused on characterizing the mechanical properties and behaviors of these biological tissues and their biomaterial analogs. Such investigations are critical not only for elucidating the fundamental biomechanical principles that govern these structures but also for advancing biomedical applications, including the design of implants, prosthetics, and tissue engineering scaffolds.

To explore the intricate relationship between the

* Corresponding author
E-mail address: knarooei@kntu.ac.ir (K. Narooei)
https://doi.org/10.22099/IJMF.2024.50853.1301

mechanical properties and functional performance of cellular hard tissues like bone and scaffolds, the elastic deformation region was initially studied. The relationship between the complex hierarchical structure of bone and its mechanical properties has revealed that the rule of mixtures is insufficient for predicting the mechanical behavior of bone [1]. The hierarchical structure of bone, composed of collagen and non-collagenous proteins, hydroxyapatite minerals, and porosity, contributes to its unique mechanical characteristics. The Mori-Tanaka method has effectively predicted the elastic moduli of cortical bone, demonstrating its capability in accounting for the composite nature of bone in the elastic region [2]. The constants of the elastic stiffness tensor were determined by using ultrasonic waves in three orthogonal directions and the bone microstructure were used to determine the anisotropic axes [3]. By application of ultrasonic waves at various points, the heterogeneity of porous structures can be taken into account [4]. The difference in wave velocity between the longitudinal and radial directions allows for the determination of the longitudinal elastic modulus, ranging from 20 to 25 GPa, and the radial elastic modulus, ranging from 14 to 21 GPa [5].

As the load-bearing capacity and damage of porous materials significantly depend on plastic deformation, many studies have focused on the inelastic deformation of these materials. To investigate the plastic deformation of porous materials, both tension and compression tests should be considered simultaneously in the yield criteria of these materials [6]. Deproteinized and demineralized bones have been used to investigate the deformation behavior of the mineral and protein phases that comprise the bone constituents [7]. Deformation of the demineralized bovine femur and antler samples showed plastic deformation, while the deproteinized part exhibited a brittle state. Three-point bending tests in both dry and rehydrated conditions and compression tests were performed on elk antler, and a significant failure strain (about 80 %) was observed [8].

Recently, researchers have focused on numerical studies on biological and biomaterials to overcome the limitations of experimental tests. The Johnson-Cook hardening model has been used to account for hardening, strain rate, and temperature effects on material behavior, but a plasticity model incorporating the hierarchical structure of bone has not been considered [9]. Although bone exhibits significant plastic deformation, especially under compressive stress, elastic deformation is sometimes used to model bone fracture through linear elastic fracture mechanics (LEFM) [10]. It is worth mentioning that without appropriate plasticity models that account for bone structure and the porosity volume fraction, stress distribution cannot be accurately predicted. Moreover, considering plastic deformation challenges the assumptions of linear elastic fracture mechanics (LEFM) that were used in some research [11].

The microstructure of biological tissues and biomaterials always contains porosity, even in untreated cases. This porosity can be prominently observed in demineralized or deproteinized structures [7]. Many researchers investigated the effects of porosity on the mechanical properties and the plastic deformation of porous materials. The impact of porosity and pore shape on the elastic properties of porous ceramics, investigated using micromechanics and finite element methods, showed that the elastic modulus and Poisson's ratio decrease with increasing volume fraction of porosities [12]. Implants made from porous titanium can replace biological hard tissues due to their excellent corrosion resistance, high strength, and low density. Stress shielding can also be avoided by controlling the volume fraction of porosities [13, 14]. The Gurson model is extensively employed as the yield criterion for porous materials due to its incorporation of porosity as a critical parameter [15]. Tvergaard and Needleman further modified the Gurson model to achieve better correlation with experimental studies by incorporating the effects of void nucleation and propagation [16]. The non-slip deformation mode, non-quadratic yield surface, strain localization, and fracture of materials (particularly porous materials) necessitate the inclusion of the Lode angle in the yield surface function. It has been observed that for zero hydrostatic stress, the shape of the yield loci of porous materials is identical to that of solid materials,

except that the size is reduced by a factor of $1-f$, where f represents the void volume fraction. However, in non-zero hydrostatic stress, the Lode angle parameter should be considered to predict more accurate results [17].

The J_2 flow theory (von Mises yield surface) was utilized to obtain numerical results for the deformation of the voided unit cell. The Gurson yield function, influenced by the Lode angle, was then employed to achieve similar results without considering the porosities in the geometry of the unit cell [18]. Utilizing the Hershey-Hosford yield criterion to account for the plastic deformation of the porous material matrix demonstrated that the yield loci on the deviatoric plane show a transition from a hexagon to a rounded triangle or the circular shape described by the Gurson criterion, depending on the stress triaxiality [19]. Some researchers have considered the mechanical behavior of porous materials by assuming the porosity geometry or its effect by considering the pressure dependency of materials, while the effect of stress state has not been fully addressed [20-22]. However, it was shown that the Lode angle significantly contributes to the mechanical behavior as this parameter is sensitive to the stress state [23]. The Gurson model, while it considers the void volume fraction [24], should be enhanced with a function of the third invariant of stress tensor (Lode angle) to consider the effect of the stress state [25]. It has been shown that stress triaxiality (stress state) has a significant role in the necking and post-necking yield behavior [26]. Investigation into the plastic deformation of cement stone has shown that the Lode angle should be considered in the plastic yield function to control the deviatoric plane's shape and capture strain in the direction of intermediate principal strain [27].

Regarding previous studies, it can be concluded that porosity is not the only factor affecting the mechanical behavior of porous materials, and the stress state should be taken into account by considering the Lode angle [8]. In the current research, the Gurson yield function has been generalized to include a function of the Lode angle to account for the stress state in plastic deformation. This modified yield function has been used to predict the plastic deformation of non-uniform samples made from steel, untreated elk antler (UEA), cellular polyurethane foam (CPF), and porous hierarchical bioscaffold (PHB). According to the results, it is possible to characterize the mechanical behavior of solid to porous materials under different types in tension and compression loading. The manuscript is organized as follows: The first part outlines the theoretical framework of the research. The second part illustrates the yield surface resulting from the proposed modification of the yield function. In the final part, the results of finite element constitutive modeling are discussed and compared with experimental results.

2. Porous Plasticity Models

Many experimental studies have investigated the plastic behavior of biomaterials such as bioscaffolds and polyurethane foams. However, some researchers have considered the simulation of the plastic deformation of these materials [20, 21]. The modified Gurson model has been widely used to predict the plastic deformation of porous materials under mechanical loading. As experimental reports disproved the volume-preserving assumption of porous biological materials during plastic deformation [8, 21], the modified Gurson model has been used to determine the yield surface as follows [15, 16]:

$$\phi = \left(\frac{\sigma_{eq}^{VM}}{\sigma_M}\right)^2 + 2fq_1\cosh\left(\frac{3}{2}q_2\frac{\sigma_h}{\sigma_M}\right) - 1 - (fq_1)^2 = 0 \quad (1)$$

Where $\sigma_{eq}^{VM} = \sqrt{\frac{3}{2}\boldsymbol{S}:\boldsymbol{S}}$ is the von Mises effective stress (where $\boldsymbol{S}$ represents the deviatoric stress tensor and : shows double dot contraction), σ_M is the yield strength of the fully dense matrix, σ_h stands for the hydrostatic stress, and f represents the porosity volume fraction. It is worth mentioning that the well-known von Mises yield criterion can be derived from Eq. (1) when $f=0$. Tvergaard and Needleman determined the coefficients $q_1 = 1.5$ and $q_2 = 1$ to achieve the best correlation with the simulation results of a unit cell

containing voids [15, 16]. It was observed that, due to the stress heterogeneity imposed by voids, yield functions typically exhibit a dependency on the third stress invariant [22]. However, in classical plasticity, the dependency of the yield function on the third invariant has been neglected. The Lode angle is defined to account for the third invariant of the stress tensor as follows [19]:

$$\theta = \frac{1}{3}\arccos\left(\frac{27}{2}\frac{J_3'}{{\sigma_{eq}^{VM}}^3}\right) \tag{2}$$

Where $J_3' = \det(\boldsymbol{S})$ represents the third invariant of the deviatoric stress tensor ($\boldsymbol{S}$). The non-quadratic equivalent stress is defined as [17]:

$$\begin{aligned}\sigma_{eq} = \Bigg[\frac{1}{2}\big((\sigma_1-\sigma_2)^m + (\sigma_1-\sigma_3)^m \\ + (\sigma_2-\sigma_3)^m\big)\Bigg]^{\frac{1}{m}} \\ = \sigma_{eq}^{VM} g(\theta)\end{aligned} \tag{3}$$

As seen from Eq. (3), it is insightful to express the effective stress as the product of the von Mises effective stress and a function of the Lode angle, $g(\theta)$.

The Hershey-Dalgreen-Hosford yield function (ϕ) is an extension of the von Mises yield function with the following formulation of the Lode angle [17]:

$$\begin{aligned}&\phi = \sigma_{eq}^{VM} g(\theta) - \sigma_M = 0 \\ &g(\theta) = \frac{2}{3}\Bigg[\frac{1}{2}\Bigg(\Big[\cos(\theta) - \cos\Big(\theta - \frac{2\pi}{3}\Big)\Big]^m \\ &\qquad + \Big[\cos\Big(\theta - \frac{2\pi}{3}\Big) \\ &\qquad - \cos\Big(\theta + \frac{2\pi}{3}\Big)\Big]^m \\ &\qquad + \Big[\cos(\theta) \\ &\qquad - \cos\Big(\theta + \frac{2\pi}{3}\Big)\Big]^m\Bigg)\Bigg]^{\frac{1}{m}}\end{aligned} \tag{4}$$

Here, m represents an integer that should be obtained from experimental data. Similarly, Willam and Warnkle introduced the following function for $g(\theta)$ [23]:

$$g(\theta) = \frac{4(1-\beta^2)\cos^2\left(\frac{\pi}{3}-\theta\right) + (2\beta-1)^2}{2(1-\beta^2)cos\left(\frac{\pi}{3}-\theta\right) + (2\beta-1)\sqrt{4(1-\beta^2)\cos^2\left(\frac{\pi}{3}-\theta\right) + \beta(5\beta-4)}} \tag{5}$$

Where, β is an adjusting parameter used to align the model with experimental data. In this research, the extension of the von Mises yield function for the porous material was used [17, 19]:

$$\phi = \sigma_{eq}^{VM} g(\theta) - (1-f)\sigma_M = 0 \tag{6}$$

As mentioned earlier, f represents the volume fraction of voids, and this yield function reduces to the yield function of Eq. (4) for fully dense material when $f = 0$. Considering the modification of Eq. (3) (the non-quadratic form of effective stress σ_{eq}), the new form of the Gurson model can be defined to include the Lode angle (third invariant of deviatoric stress) as [18, 19]:

$$\begin{aligned}\phi = \left(\frac{\sigma_{eq}}{\sigma_M}\right)^2 + 2fq_1\cosh\left(\frac{3}{2}q_2\frac{\sigma_h}{\sigma_M}\right) - 1 - (fq_1)^2 \\ = 0\end{aligned} \tag{7}$$

Since σ_M represents the instantaneous yield strength of the matrix (fully dense material), the hardening or softening during plastic deformation must be defined by an appropriate stress-strain relationship. This relationship should typically be calibrated using uniaxial tension and compression tests, especially for pressure-dependent materials. In the current research, we used the Voce model that relates the matrix yield strength (σ_M) to the effective plastic strain ($\bar{\varepsilon}$) as follows [18]:

$$\sigma_M = A + B(1 - Ce^{D\bar{\varepsilon}}) \tag{8}$$

Where A, B, C, and D are material parameters that should be defined by the fitting to the experimental data. The deformation mode can alter the void volume fraction, and the volume fraction increment proposed in [18, 24] is modified here by an adjusting parameter α to control the rate of increase in the volume fraction of

porosities:

$$df = (1-f)\alpha d\varepsilon_{ii}^{p} \tag{9}$$

Where i represents the dummy index, and summation over it is implied. It is worth mentioning that the parameter α is usually considered to be 1, and in exceptional cases, its specific value will be noted in the context. The plastic strain tensor $\boldsymbol{\varepsilon}^{p}$ is defined by the flow rule as:

$$d\boldsymbol{\varepsilon}^{p} = d\lambda \frac{\partial \phi}{\partial \sigma} \tag{10}$$

In Eq. (10), $d\lambda$ is a scalar parameter, and σ represents the stress tensor. Although Eq. (9) can be evaluated numerically, with the simplifying assumption that the plastic strain is not affected by the void volume fraction, Eq. (9) can be integrated as follows:

$$f = 1-(1-f_0)e^{-\alpha\varepsilon_{ii}^{p}} \tag{11}$$

Here, f_0 represents the initial volume fraction of porosities.

In the following sections, we aim to identify the most suitable yield surface that corresponds to the experimental data of a non-uniform sample made from steel, untreated elk antler (UEA), cellular polyurethane foam (CPF), and porous hierarchical bioscaffold (PHB). This analysis will take into account the porosity of their microstructures and their observed mechanical behavior. In the first step, the resulting yield loci were plotted by considering Eqs. (4) to (7) in Maple software. To simulate the response of samples to mechanical loading, COMSOL Multiphysics was programmed to consider Eqs. (4) to (7). Linear elements and symmetry boundary conditions were used in all simulations due to the geometry of the investigated samples (see Figs. 5 and 8). In the uniaxial test simulation, the tensile boundary condition was imposed on the loaded edge and in the compression test simulations, contact with a rigid platen was considered (see Fig. 8).

3. Materials

In the first step, the modified von Mises yield criterion incorporating the Lode angle was studied in the uniaxial tension of Chinese steel Q235B [25]. Additionally, an untreated elk antler [7], a porous hierarchical bioscaffold (used for bone regeneration) [20], and a cellular polyurethane foam (for simulating trabecular bone) [21] were used to justify the modified Gurson yield surfaces. The coefficients of the Voce model, derived from fitting to the plastic deformation data reported in the literature, along with the dimensions of the finite element (FE) analysis for the simulated sample, were presented in Table 1. The results of the fittings, performed using a Python code that utilizes the curve fitting function from the SciPy library, can be seen in Fig. 1.

4. Results and Discussion

Researchers are keen to find a yield surface that can predict the yield behavior of various materials. By combining Eqs. (5) and (6) and considering $0.5 \leq \beta \leq 1$ to ensure the convexity of the yield surface [17], different shapes of the yield surface are obtained, as shown in Fig. 2. In the following discussion, non-dimensional stress axes are used to represent the yield locus (or surface) by normalizing the stresses with the yield strength (Y). It is observed that although different yield loci predict similar yielding under uniaxial loading, they exhibit varied behavior under other loading modes. Therefore, it is possible to determine an appropriate yield surface for different materials by adjusting the β parameter and the void volume fraction. In Fig. 2, for $\beta = 1$ the von Mises yield surface can be captured, and it can be observed that similar stress magnitudes produce yielding in both uniaxial and balanced biaxial loadings. Additionally, by varying the β parameter, different balanced biaxial tension in plastic deformation can be captured. Moreover, it is evident that balanced biaxial compression remains unchanged for different β parameters, in contrast to balanced biaxial tension. This is particularly interesting in the compression mode, as higher yield strength is expected in this mode, especially for pressure-dependent materials.

Table 1. Mechanical properties and test sample size of untreated elk antler [7], porous hierarchical bioscaffold [20], cellular polyurethane foam [21], and steel Q235B [25]

	A **(MPa)**	***B*** **(MPa)**	***C***	***D***	**Sample size (mm^3)**
Untreated elk antler (UEA) [7]	8.54	5.92	-1.02×10^{-2}	-30.22	7.5 × 5 × 5
Porous hierarchical bioscaffold (PHB) [20]	21.04	31.94	-5.07	280	7.5 × 5 × 1
Cellular polyurethane foam (CPF) [21]	1.72	1.31	1.38	30.45	8 × 8 × 8
Q235B steel [25]	250.58	261.41	-1.07	15	90 × 40 × 3

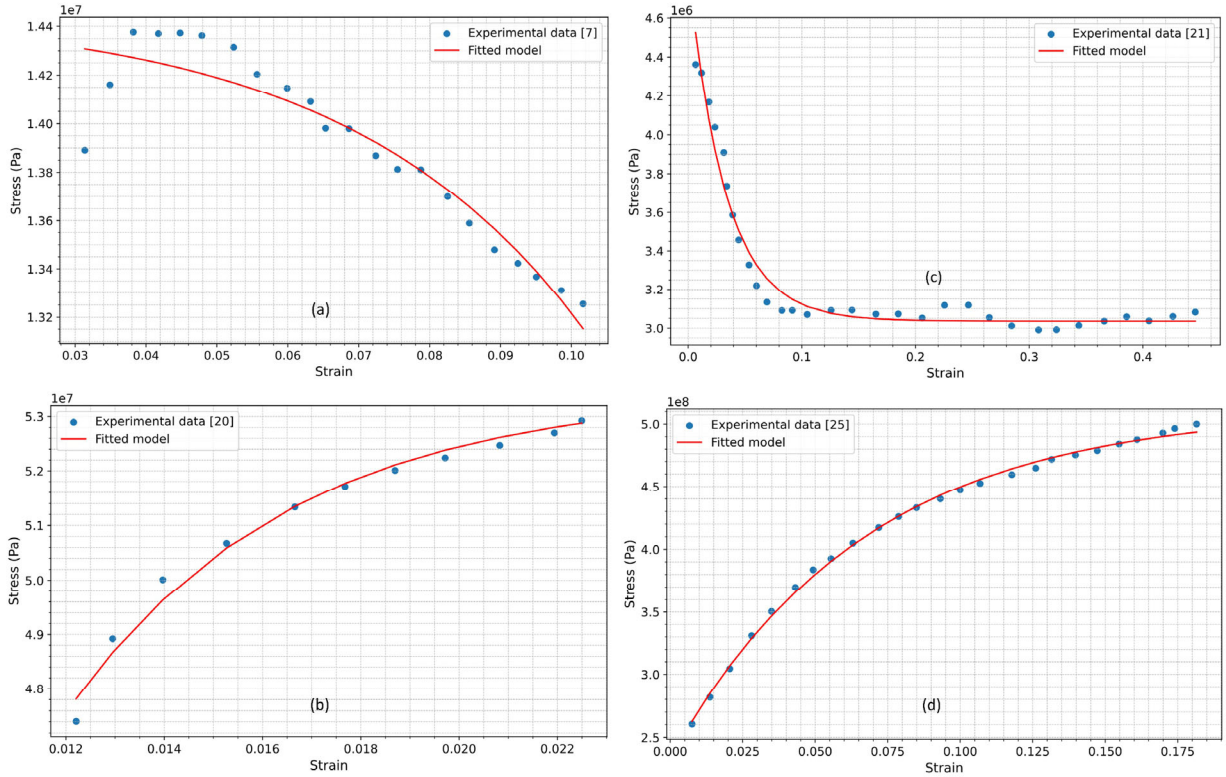

Fig. 1. Results of Voce model fitting with experimental data of (a) elk antler [7], (b) porous hierarchical bioscaffold [20], (c) cellular polyurethane foam [21], and (d) Q235B steel [25].

By considering the same yield function (Eq. (6)) and only changing the $g(\theta)$ function (Eq. (4)), different yield loci can be obtained, as shown in Fig. 3 (Hershey-Dalgreen yield surface). As seen for $m = 1$, the Tresca yield locus can be obtained; additionally, as m increases, the yield loci approach the Tresca yield locus again. This demonstrates that different yield loci can be achieved by simply altering the yield function parameters. Comparing Figs. 2 and 3 reveals that the Hershey-Dalgreen yield loci represent similar behavior for the uniaxial and balanced biaxial modes, in contrast to the Willam-Warnke yield function.

The Gurson model has been successfully used to predict the mechanical behavior of porous materials [24]. As previously mentioned, the third invariant, or equivalently, the Lode angle, influences the plastic deformation of porous media because the stress state significantly affects the plastic deformation. Therefore, Eqs. (4) and (7) were used to construct the modified Gurson yield function, and the yield loci for different m values can be seen in Fig. 4. The case of zero porosity volume fraction in Eq. (7) is equivalent to the von Mises yield criterion, and thus $f = 0.1$ was considered here. From Fig. 4, it can be observed that the uniaxial and balanced biaxial modes coincide for different m parameters. As $m \to \infty$, the yield loci approach a

hexagon with smooth apices.

In the tension of a uniform specimen, the tensile stress is uniformly distributed across the entire sample before necking occurs. In this case, the stress-strain experimental data can be fitted using the Voce model, as shown in Fig. 1. The experimental data can typically be captured using finite element constitutive modeling by choosing a yield criterion for the plastic mechanical behavior, such as the von Mises criterion. However, when a non-uniformity is introduced into the geometry of the samples, it is expected that the experimental data for this geometry can still be accurately captured by finite element modeling. However, as the geometrical non-uniformity disrupts the uniaxial stress state in the tension test, this expectation is not met. To address this issue, we used the experimental data on the standard tensile specimen from Q235B steel [25] to fit with the Voce model (Table 1 and Fig. 1(d)). These data were used to simulate the tensile behavior of a non-uniform geometry in the tensile deformation (Fig. 5), and comparison between the experimental [25] and simulated results can be seen in Fig. 6. From Fig. 6(a), it can be observed that due to the change in the stress state in the non-uniform sample, the von Mises yield criterion ($m = 2$) cannot accurately predict the experimental data. By adjusting the m value to $m = 12$, the experimental data in the plastic regime can be captured accurately.

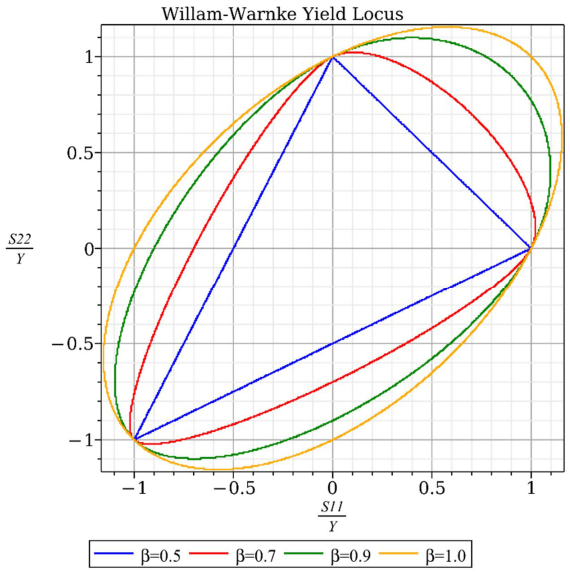

Fig. 2. Willam-Warnke yield locus at different β parameters of Eq. (5) and $f = 0$ in Eq. (6).

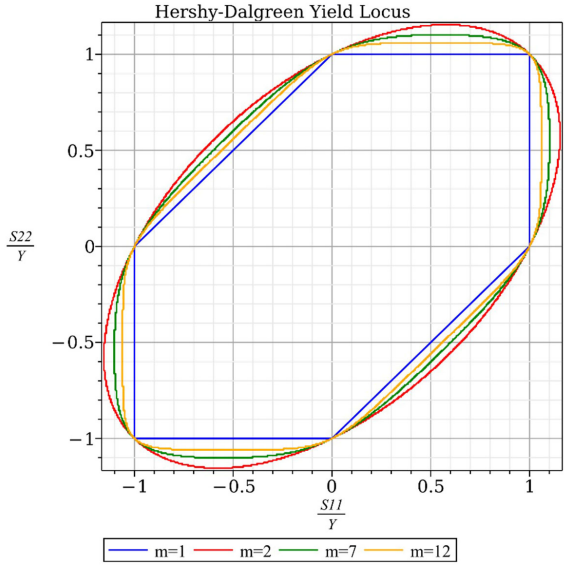

Fig. 3. Hershy-Dalgreen yield locus at different m parameters of Eq. (4) and $f = 0$ in Eq. (6).

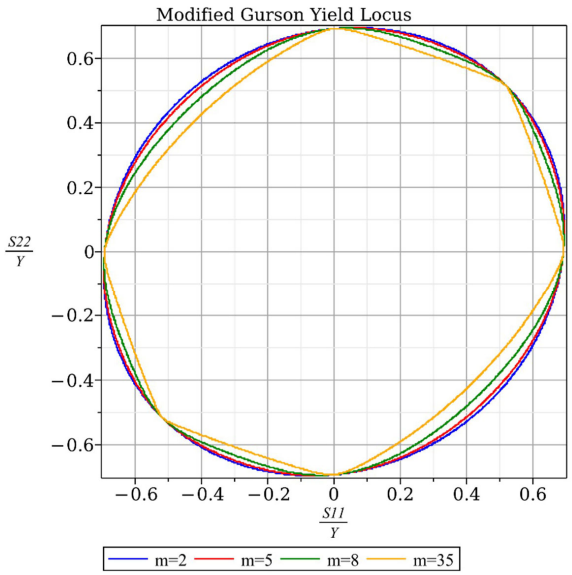

Fig. 4. Modified Gurson yield loci at different m parameters of Eq. (4) and $f = 0.1$ in Eq. (7).

This agreement is attributed to the shear stresses in this geometry, in contrast to the uniform samples, which lead to non-uniform stress and strain distribution, as can be seen in Figs. 6(b) and 6(c).

The cortical (compact) and cancellous (trabecular) bones are the two main parts of bone, with the density and morphology of the cancellous part depending on the applied stress [7]. From another perspective, polyurethane (PU) foam can be used to simulate trabecular bone [21].

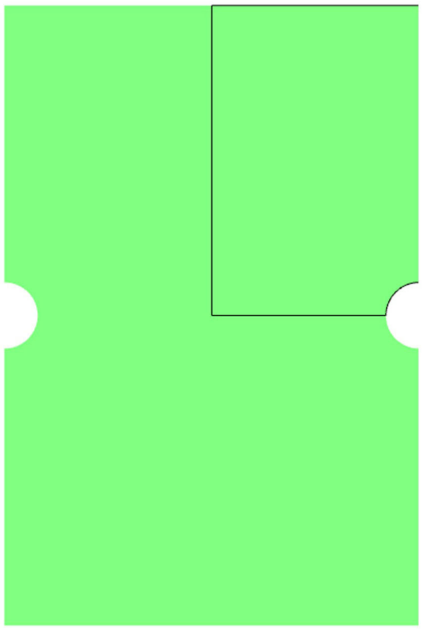

Fig. 5. Non-uniform tensile specimen with dimension 265 × 40 × 3 mm^3 and necking radius of 10 mm.

Thereby, the mechanical behavior of bone and PU foam was investigated, as mentioned earlier, from both constitutive modeling and experimentally. The stress state, such as tension or compression, plays a significant role in the plastic deformation of porous and cellular materials. The modified Gurson model was applied to the elk antler ($m = 16$), PU foam ($m = 8$), and bovine cortical bone bioscaffold ($m = 16$) by taking into account the Voce hardening model (Table 1). The results of the stress-strain behavior in compression loading for different relative densities of elk antler, PU foam, and bovine cortical bone bioscaffold can be seen in Fig. 7. Fig. 7(a) shows that with increasing relative density, the material strength also increases. In the stress-strain curve, initial hardening is observed due to a decrease in void volume fraction in the compressive stress state. After sufficient densification, the rate of strain softening of the solid matrix (Fig. 1(a)) exceeds the hardening rate due to decreasing porosity. It can be seen that the trend of the curves follows the experimental data, indicating that the Lode dependency of the yield function has a suitable form. Other hardening models can be used to better agree with experimental data, especially at higher densities, but this is not the scope of the current research. Bioscaffolds are usually porous, as they are candidates for tissue regeneration, and they must also provide sufficient mechanical support. In the previous research, the hierarchical structure of the scaffold was considered in the geometry of the simulated sample [20]. Due to the complex geometry of the scaffold, this method can only be used in a representative volume element (RVE) of the material. Therefore, computation is feasible only on a small-scale RVE, not a macro sample. In the current research, we considered the porosity as a parameter in the proposed yield function and the current formulation was applied to a regular (non-porous) geometry in the simulations. The results of sample tension for a 55% porosity can be seen in Fig. 7(b), and a good agreement can be seen between the simulation and experimental data. Therefore, by selecting a suitable yield function, the deformation of complex microstructure-based materials can be simulated on a macro scale with similar results. It is worth mentioning that in previous research, micro-CT reconstructed the RVE geometry, and this method cannot be used to scaffold on a macro-scale, while the current formulation can be used on any scale.

Polyurethane (PU) foam represents a behavior similar to trabecular bone and is often used in biomechanical tests. The mechanical behavior of PU foam was studied using the modified Gurson model and Voce hardening model. As seen in Fig. 1(c), the stress-strain data from peak stress to steady stress in the plastic deformation region was used to obtain the Voce model parameters. As a wide variety of PU foams, from solid to cellular types, are used in tests, to accommodate the test data, α in Eq. (11) was considered equal to 0.2. As the Voce model overestimates the peak stress in Fig. 1(c), the peak stress in Fig. 7(b) also shows higher values. However, in the softening region, the proposed model can accurately capture the mechanical behavior of PU foam. By comparing Figs. 6(a), 7(a), and 7(b), it can be seen that the current model can be used for metals, bone, and foams with both hardening and softening behavior. To the best of our knowledge, this is the first time that a plasticity model has been applied to such a wide variety of materials.

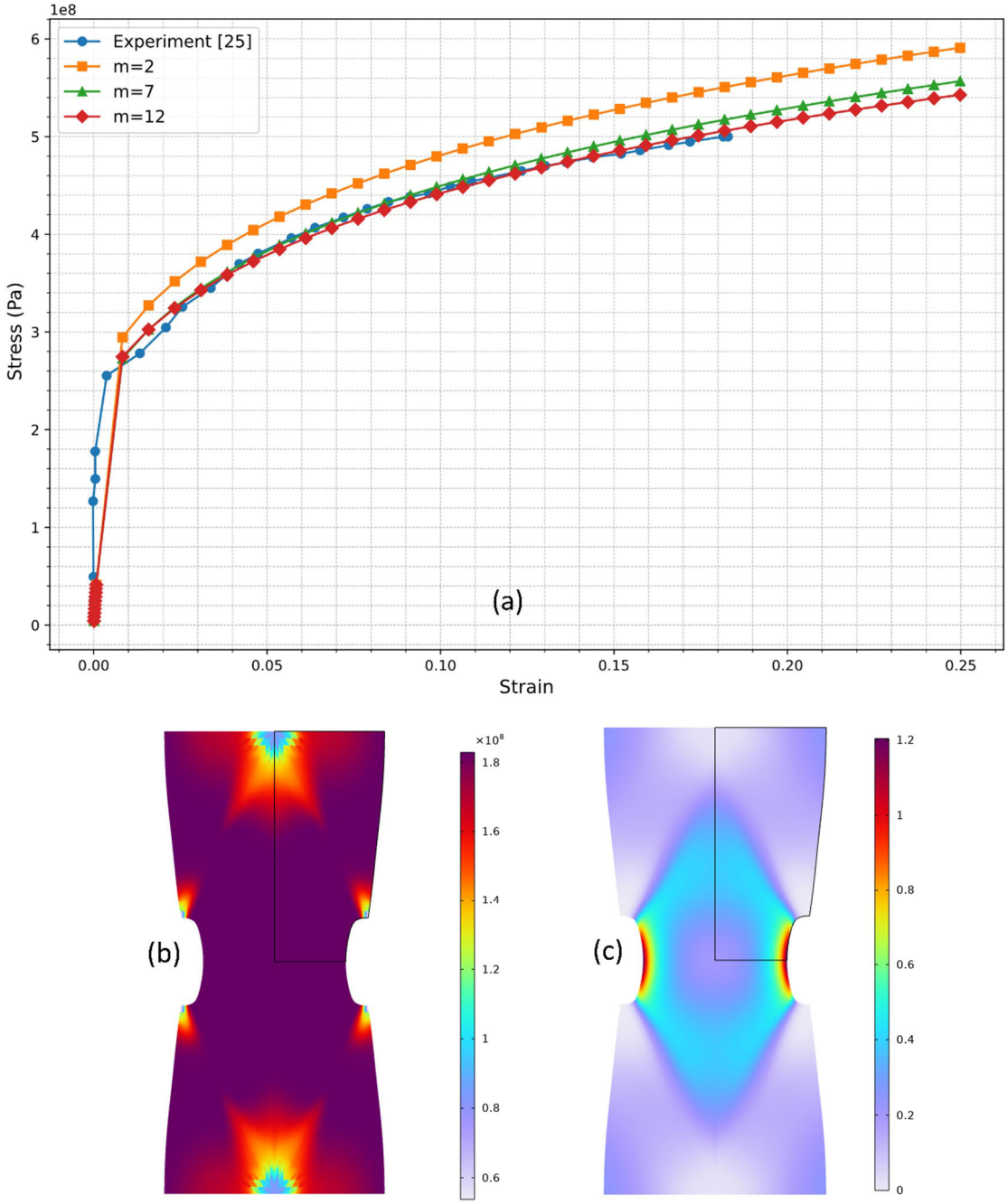

Fig. 6. (a) Comparison between simulated and experimental data [25] for non-uniform geometry of Fig. 5, (b) stress (Pa), and (c) strain distribution in tension of non-uniform specimen.

It is understood that barreling in the compression test occurs due to friction and usually leads to the formation of shear bands in compressed specimens. However, the appearance of barreling in porous materials can differ from that in non-porous materials. The results of PU foam compression tests for 1% porosity and 40% porosity, with a Coulomb friction coefficient of 0.1, can be seen in Fig. 8. By comparing Figs. 8(a) and 8(b), it can be concluded that with an increase in the porosity volume fraction, the barreling decreases. As can be seen from Figs. 8(a) and 8(b), this reduction is attributed to the increased compressibility of the material as the porosity level rises.

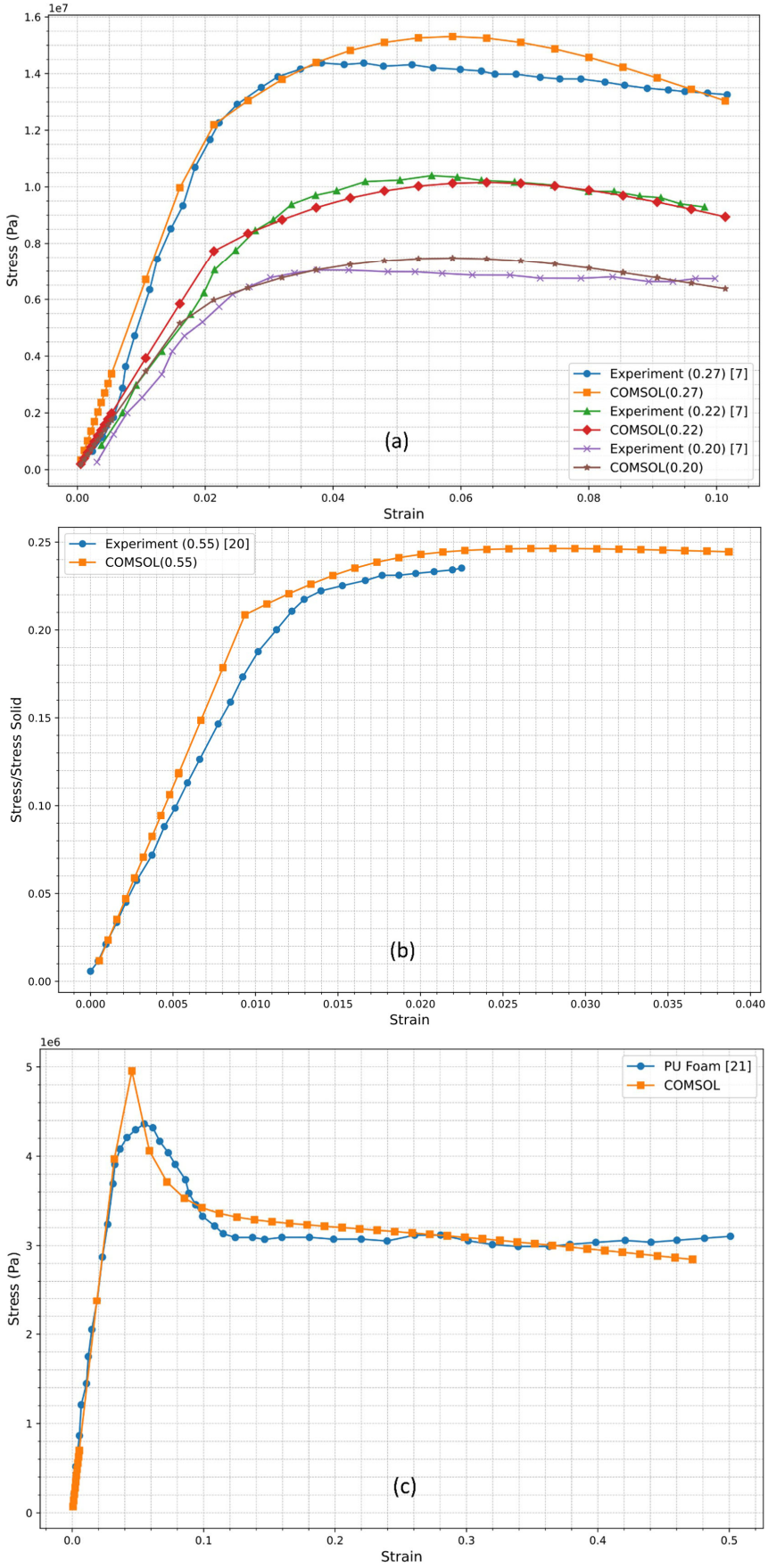

Fig. 7. Comparison between simulated and experimental data of (a) elk antler, (b) bovine cortical bioscaffold, and (c) PU foam.

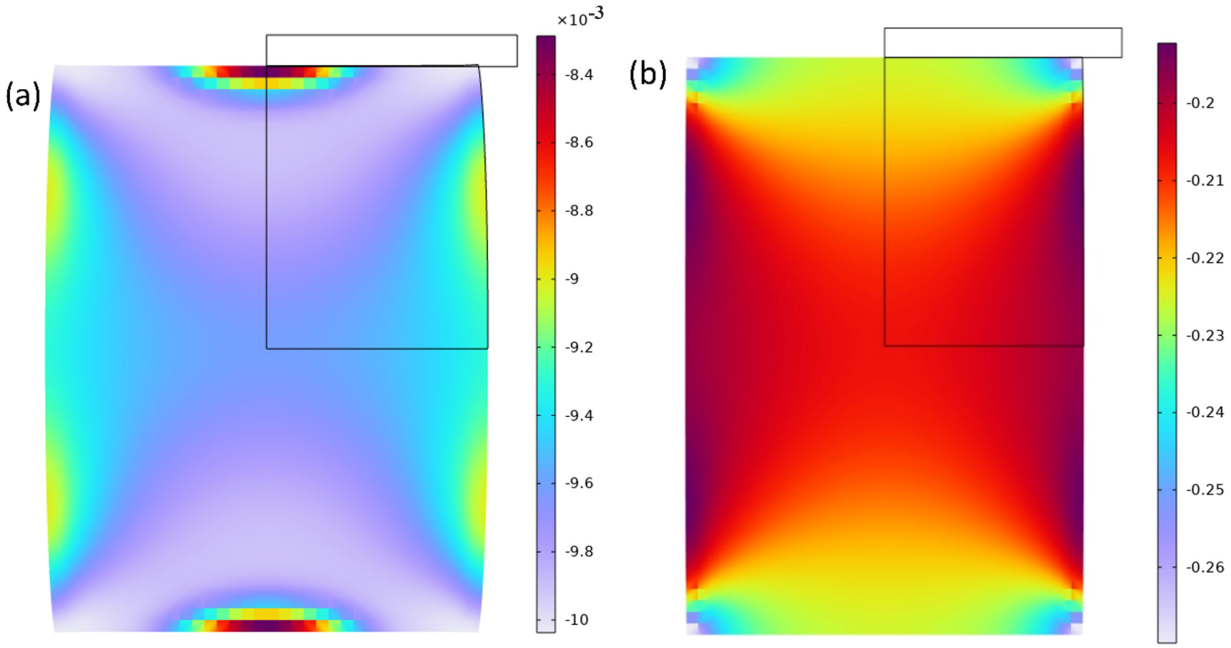

Fig. 8. Volumetric plastic strain and barreling appearance: (a) 1% porosity and (b) 40% porosity.

5. Conclusion

It is well known that the Lode angle accounts for the stress state, and in this work, its influence on the plastic deformation of dense and porous materials was considered. To model the mechanical behavior of widespread materials using plasticity models, the von Mises and Gurson yield functions were multiplied by a function of the Lode angle. The Voce model was invoked to consider the hardening/softening of materials in the uniaxial test. The material parameters of the Voce model were extracted by fitting them to the experimental data. Results showed that extensive yield loci can be obtained by changing the Lode function parameters, while without considering the Lode angle's function, the yield locus's shape does not change.

A comparison of the uniaxial tension test on the non-uniform geometry of samples showed that the Lode angle should be taken into account as the stress distribution in the sample is not uniform. It was observed that to accurately model the mechanical behavior of elk antler, the Gurson model can be used with a function of the Lode angle, as the porosity in the antler creates pressure-dependent materials, and in this case, the stress state during plastic deformation must be considered. Results from bioscaffold modeling demonstrated that instead of using a complex geometry at the microscale, the current formulation can be applied on a non-porous sample, with the effects of porosity (microstructure) accounted for by the volume fraction of porosities. The results of compressing porous PU foam showed that the appearance of barreling depends on both friction and porosity, in contrast to solid materials, which depend only on friction. Finally, we hope that future research will lead to the proposal of a general yield function capable of addressing the plastic deformation of various materials rather than relying on multiple proposed yield functions.

Acknowledgments

The author expresses his gratitude to the research board of K. N. Toosi University of Technology for their financial support and provision of research facilities utilized in this study.

Conflict of interest

The author declares that there is no conflict of interest in this research.

Funding

The author declares that no funds, grants, or other support were received during the preparation of this manuscript.

6. References

[1] Rho, J. Y., Kuhn-Spearing, L., & Zioupos, P. (1998). Mechanical properties and the hierarchical structure of bone. *Medical Engineering & Physics, 20*(2), 92-102. https://doi.org/10.1016/s1350-4533(98)00007-1

[2] Hamed, E., Novitskaya, E., Li, J., Chen, P. Y., Jasiuk, I., & McKittrick, J. (2012). Elastic moduli of untreated, demineralized and deproteinized cortical bone: validation of a theoretical model of bone as an interpenetrating composite material. *Acta Biomaterialia, 8*(3), 1080-1092. https://doi.org/10.1016/j.actbio.2011.11.010

[3] Orías, A. A. E. (2005). *The relationship between the mechanical anisotropy of human cortical bone tissue and its microstructure* [Doctoral dissertation, University of Notre Dame]. https://doi.org/10.7274/9k41zc79t6t

[4] Pithioux, M., Lasaygues, P., & Chabrand, P. (2002). An alternative ultrasonic method for measuring the elastic properties of cortical bone. *Journal of Biomechanics, 35* (7), 961-968. https://doi.org/10.1016/S00219290(02)00027-1

[5] Lasaygues, P., & Pithioux, M. (2002). Ultrasonic characterization of orthotropic elastic bovine bones. *Ultrasonics, 39*(8), 567-573. https://doi.org/10.1016/S0041-624X(02)00261-5

[6] Mercer, C., He, M., Wang, R., & Evans, A. (2006). Mechanisms governing the inelastic deformation of cortical bone and application to trabecular bone. *Acta Biomaterialia, 2*(1), 59-68. https://doi.org/10.1016/j.actbio.2005.08.004

[7] Chen, P. Y., & McKittrick, J. (2011). Compressive mechanical properties of demineralized and deproteinized cancellous bone. *Journal of the Mechanical Behavior of Biomedical Materials, 4*(7), 961-973. https://doi.org/10.1016/j.jmbbm.2011.02.006

[8] Chen, P. Y., Stokes, A., & McKittrick, J. J. A. B. (2009). Comparison of the structure and mechanical properties of bovine femur bone and antler of the North American elk (Cervus elaphus canadensis). *Acta Biomaterialia, 5*(2), 693-706. https://doi.org/10.1016/j.actbio.2008.09.011

[9] Alam, K., Mitrofanov, A. V., Bäker, M., & Silberschmidt, V. V. (2009, August). Stresses in ultrasonically assisted bone cutting. In *Journal of Physics: Conference Series* (Vol. 181, No. 1, p. 012014). IOP Publishing. https://doi.org/10.1088/1742-6596/181/1/012014

[10] Huang, J., Rapoff, A. J., & Haftka, R. T. (2006). Attracting cracks for arrestment in bone-like composites. *Materials & Design, 27*(6), 461-469. https://doi.org/10.1016/j.matdes.2004.11.022

[11] Sugita, N., Osa, T., Aoki, R., & Mitsuishi, M. (2009). A new cutting method for bone based on its crack propagation characteristics. *CIRP Annals, 58*(1), 113-118. https://doi.org/10.1016/j.cirp.2009.03.057

[12] Roberts, A. P., & Garboczi, E. J. (2000). Elastic properties of model porous ceramics. *Journal of the American Ceramic Society, 83*(12), 3041-3048. https://doi.org/10.1111/j.1151-2916.2000.tb01680.x

[13] Nakajima, H., & Ide, T. (2018). Fabrication, properties and applications of porous metals with directional pores. M*aterials Science Forum, 933*, 49-54. https://doi.org/10.1016/j.pmatsci.2006.09.001

[14] Gibson, L., & Ashby, M. (1997). *Cellular solids: structure and properties*. Cambridge University Press.

[15] Tvergaard, V. (1981). Influence of voids on shear band instabilities under plane strain conditions. *International Journal of Fracture, 17*(4), 389-407. https://doi.org/10.1007/BF00036191

[16] Tvergaard, V., & Needleman, A. (1984). Analysis of the cup-cone fracture in a round tensile bar. *Acta Metallurgica, 32*(1), 157-69. https://doi.org/10.1016/0001-6160(84)90213-X

[17] Benallal, A. (2017). Constitutive equations for porous solids with matrix behaviour dependent on the second and third stress invariants. *International Journal of Impact Engineering, 108*, 47-62. https://doi.org/10.1016/j.ijimpeng.2017.05.004

[18] Dæhli, L. E., Morin, D., Børvik, T., & Hopperstad, O. S. (2018). A Lode-dependent Gurson model motivated by unit cell analyses. *Engineering Fracture Mechanics, 190*, 299-318. https://doi.org/10.1016/j.engfracmech.2017.12.023

[19] Dæhli, L. E. B., Hopperstad, O. S., & Benallal, A. (2019). Effective behaviour of porous ductile solids with a non-quadratic isotropic matrix yield surface. *Journal of the Mechanics and Physics of Solids, 130*, 56-81. https://doi.org/10.1016/j.jmps.2019.05.014

[20] Huang, S., Li, Z., Chen, Z., Chen, Q., & Pugno, N. (2013). Study on the elastic–plastic behavior of a porous hierarchical bioscaffold used for bone regeneration. M*aterials Letters, 112*, 43-46. https://doi.org/10.1016/j.matlet.2013.08.114

[21] Kelly, N., & McGarry, J. P. (2012). Experimental and numerical characterization of the elasto-plastic properties of bovine trabecular bone and a trabecular bone analogue. *Journal of the Mechanical Behavior of Biomedical Materials, 9*, 184-97.

https://doi.org/10.1016/j.jmbbm.2011.11.013

[22] Cazacu, O., & Revil-Baudard, B. (2015). New three-dimensional plastic potentials for porous solids with a von Mises matrix. *Comptes Rendus Mécanique, 343*(2), 77-94. https://doi.org/10.1016/j.crme.2014.12.001

[23] Willam, K. J., & Warnke, E. (1975). Constitutive model for the triaxial behaviour of concrete. *International Association for Bridge and Structural Engineering Proceedings, 19*, 1-30. https://sid.ir/paper/600004/en

[24] Ansari Basir, E., & Narooei, K. (2016). Simulation of deformation behavior of porous titanium using modified Gurson yield function. *Iranian Journal of Materials Forming, 3*(2), 26-38. https://doi.org/10.22099/ijmf.2016.3861

[25] Dong, Y., & Jia, L. J. (2021). Plasticity model for structural steel with Lode angle dependence. *Journal of Bridge Engineering, 26*(12), 04021087. https://doi.org/10.1061/(ASCE)BE.1943-5592.0001784

[26] Milone, A., Foti, P., Berto, F., & Landolfo, R. (2024). Post-necking and damage modelling of steel structural components: A comprehensive state of the art. *Engineering Structures, 321*, 118931. https://doi.org/10.1016/j.engstruct.2024.118931

[27] Liu, J., Li, X., Wang, C., Xu, Y., & Xia, K. (2024). A three-dimensional elastoplastic constitutive model incorporating Lode angle dependence. *Geomechanics for Energy and the Environment*, *38*, 100567. https://doi.org/10.1016/j.gete.2024.100567